

General paper

MICROCRACKING BEHAVIOR AND LIFE LAW OF FATIGUE IN A CAST TiAl INTERMETALLIC COMPOUND AT HIGH TEMPERATURE

Mitsuyoshi TSUTSUMI*, Ryuichi OHTANI*, Takayuki KITAMURA* and
Shin-ichi TAKANO**

*Department of Engineering Physics and Mechanics,
Graduate School of Engineering, Kyoto University, Kyoto 606-01, Japan

**Nikki Co., Ltd., Tokyo 100, Japan

Abstract: In order to elucidate the fracture process in high-temperature low-cycle fatigue of a cast Ti-34wt.%Al with lamellar structure and to derive the life law of smooth specimens, the behavior of initiation and growth of microcracks is observed in detail. The results obtained are summarized as follows. (1) Microcracks, which originate from casting defects at and/or beneath the specimen surface, begin to initiate at less than 15% of the failure life. (2) The transgranular microcracks grow perpendicularly to the stress axis and transversely to the lamellar boundaries. They are neither blocked nor decelerated by the grain boundary. (3) Although the growth rate of microcracks has a large scatter, the average rate coincides with the fracture mechanics law which is characterized by the relationship between the crack growth rate, dc/dN , and the fatigue J-integral range, ΔJ_f . (4) The crack initiating at the earliest stage of many distributed cracks tends to grow up to be a main crack for the failure. (5) The fatigue life of smooth specimens, N_f , is successfully correlated with $\Delta \sqrt{W_f}$ -parameter which is derived by integrating fracture mechanics law of dc/dN vs. ΔJ_f relation.

Key words: Intermetallic compound, TiAl, High temperature fatigue, Fatigue life, Microcrack, Crack initiation, Crack growth, $\Delta \sqrt{W_f}$ -parameter

1. INTRODUCTION

Because of high relative strength and heat resistance, the TiAl intermetallic compound is one of the most promising materials for high temperature use. Especially, a deep interest is taken in a TiAl with $\gamma+\alpha_2$ lamellar structure, as it possesses superior mechanical properties [1,2]. Although tensile or compressive properties have been investigated on the TiAl [1-5], it is more important to understand the mechanism and mechanics of fatigue failure at high temperatures in terms of practical use. However, few studies have been conducted on the fatigue behavior at high temperatures [6-11]. The authors have investigated the fatigue behavior of a cast Ti-34wt.%Al such as failure lives [12,13] and macrocrack growth including creep effect [14] at high temperatures as well as room temperature.

The objective of this paper is to investigate the fracture process of the cast TiAl in high-temperature low-cycle fatigue (LCF) and to derive its life law. As it has been clear that the initiation and growth of microcracks govern the LCF fracture of metallic materials in general, a focus is put on the characteristics of microcracks paying attention to the microstructural factors such as the effect of casting defects, lamellar boundaries and grain boundaries.

2. EXPERIMENTAL PROCEDURE

The material tested is a polycrystalline Ti-34wt.%Al of

which chemical composition is listed in Table 1. It was cast into a columnar ingot in argon gas by the plasma-skull melting process. Grains grew from the circumference to the center in the ingot during the solidification so that the elongated grains were formed as schematically illustrated in Fig.1. The average grain sizes are 3mm in the growth direction and 350 μm in the transverse one, respectively. Neither heat treatment nor HIP (Hot Isostatic Press) treatment is applied but it is tested as cast. The lamellae composed of γ -phase (TiAl) and α_2 -phase (Ti₃Al) are formed in the grains, being perpendicular to the grain growth direction as shown in Fig.2. The inspection on the vertical cross section reveals that the material contains 2.5 small casting defects per area of 1mm² in average and 99% of them are smaller than 30 μm in the diameter. The smooth round bar specimens, of which shape and size are shown in Fig.3, are cut from the circumference near the ingot surface so that their axis are nearly parallel to the lamellar boundaries.

The strain-controlled push-pull fatigue tests are carried out at 1073K in air by means of a closed-loop, electrohydraulic servo-controlled fatigue testing machine with an induction heating device. The strain is measured by attaching the tips of extensometer to the specimen surface in the gage length of 10mm. The four tests are conducted under a triangular strain waveform with the strain rate of 1.0%/s at different total strain ranges as listed in Table 2. Since the time-dependent deformation scarcely takes place in the present tests, the creep does not affect the

fatigue fracture.

Test 2 is interrupted at the interval of every 100 cycles and the oxide film on the specimen surface is carefully removed by diamond paste for the observation of microcracks. The number and the length of cracks initiated on a fixed area (300mm²) are measured by means of an optical microscope. The cracks shorter than 20μm are excluded from the observation because it is difficult to distinguish them from the remaining oxide film. The grain boundaries and lamellae are revealed by the chemical etching before and after the test in order to identify the origin of cracks and the path of their growth. The fracture morphology is observed by means of an optical microscope and a scanning electron microscope (SEM) after the tests.

3. EXPERIMENTAL RESULTS AND DISCUSSION

3.1. Strain Range vs. Number of Cycles to Failure

Figure 4 shows the fatigue life. As the TiAl is rather brittle comparing with heat resistant steels, the total strain range, $\Delta\epsilon_t$, is composed of a small amount of the plastic strain range, $\Delta\epsilon_p$. The ratio of $\Delta\epsilon_p$ to $\Delta\epsilon_t$ is listed in Table 2. The failure of specimens is brought about by transgranular cracks which grow perpendicular to the stress axis as displayed in Fig.5. The characteristics of microcracking and their relation to the fatigue life are discussed in the following sections.

Table 1. Chemical composition (wt.%).

Material	Al	C	N	O	H	Ti
Ti-34wt%Al	33.5~ 33.6	0.01	0.003~ 0.005	0.110~ 0.114	0.0021 ~ 0.0027	Bal.

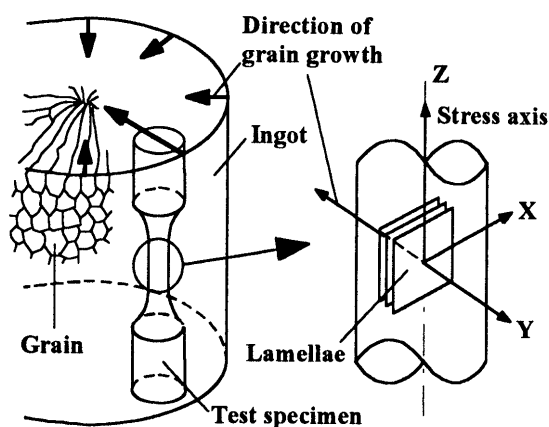


Fig.1. Schematic illustration of orientation of grain growth and lamellar formation.

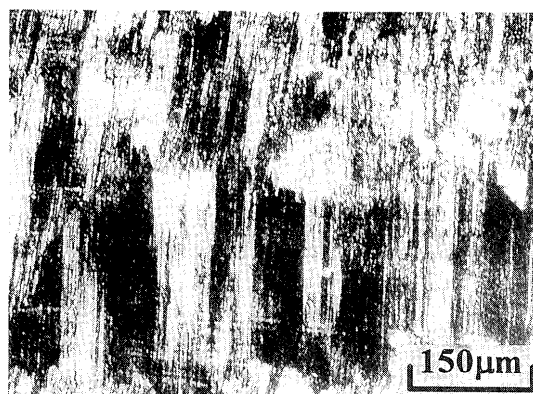


Fig.2. Microstructure of the material tested.

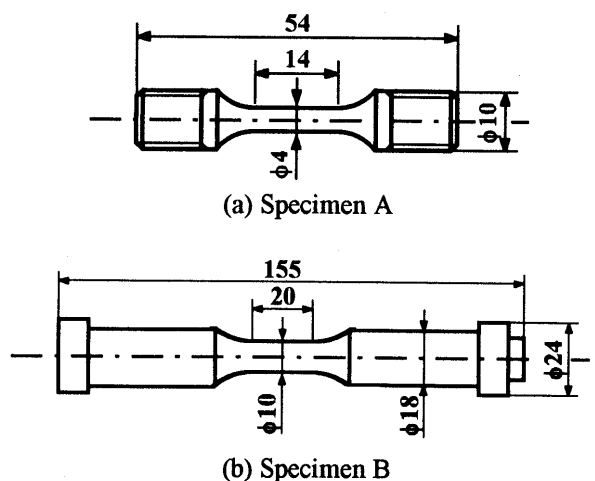


Fig.3. Shape and size of specimens (dimensions in mm).

Table 2. Test conditions.

Waveform				
	1	2	3	4
Test number	1	2	3	4
Specimen	A	B	A	A
Total strain range $\Delta\epsilon_t$, %	1.0	0.7	0.5	0.2
Plastic strain range $\Delta\epsilon_p$, %	0.355	0.181	0.052	<0.010
Ratio of $\Delta\epsilon_p$ to $\Delta\epsilon_t$	0.355	0.259	0.104	<0.05
Tensile peak stress σ_{max} , MPa	460	394	332	149
Compressive peak stress σ_{cmax} , MPa	-499	-451	-340	-155
Number of cycles to failure N_f , cycles	265	700	4905	>5 × 10 ⁶

MICROCRACKING AND LIFE LAW OF FATIGUE IN A CAST TiAl

3.2. Initiation of Microcracks

Figure 6 shows a typical feature of a microcrack at the initiation. The dark spot at the center is a casting defect from which the crack originates. All cracks observed initiate from the defects. Although the defect is not always detected on the specimen surface for some cracks, careful polishing of the surface after the test reveals a hidden defect inside the specimen. The size and location of defects which yield the crack initiation are examined for 50 sites, which are sampled at random. Removing every a few microns of surface by polishing, the shape of the defect is measured by means of a microscope and the three-dimensional shape is reconstructed. The diameter and the depth from the surface are summarized in Fig.7. The diameter is defined as the maximum length perpendicular to the stress axis, and the depth is determined as the distance between the center of defect and the original surface. It is found from Fig.7 that the cracks initiate from not only large defects but also small ones.

On the other hand, all cracks initiate from the defect whose depth is smaller than 20 μm as shown in Fig.7. The crack initiation from the defects deeper than 30 μm cannot be confirmed by the other inspection on the longitudinal cross section of all the specimens failed. Thus, the depth rather than the size is an important factor for the crack initiation. In other words, the less constraint of the deformation at the free surface enhances the fatigue fracture. The main crack which grow up to the largest crack at the failure initiates from a defect of the diameter of 25 μm on the surface (see solid symbols in Fig.7).

It has been reported that the fracture along the lamellar boundary is easy to occur in this type of TiAl [15]. However, such a lamellar delamination is not recognized in this fatigue condition because the lamellae in the present specimens are nearly parallel to the stress axis.

Figure 8 shows the change in crack density, which is

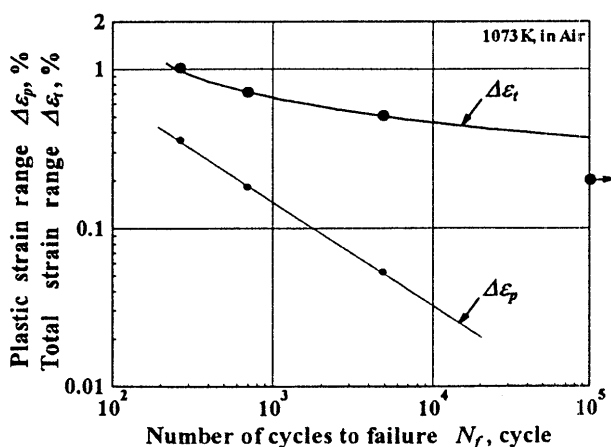


Fig.4. Fatigue life as a function of total strain range or plastic strain range.

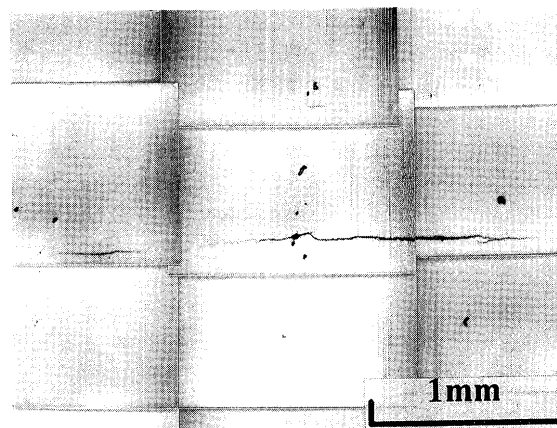


Fig.5. Morphology of surface cracks at N_f (Test 2). Stress axis is vertical.

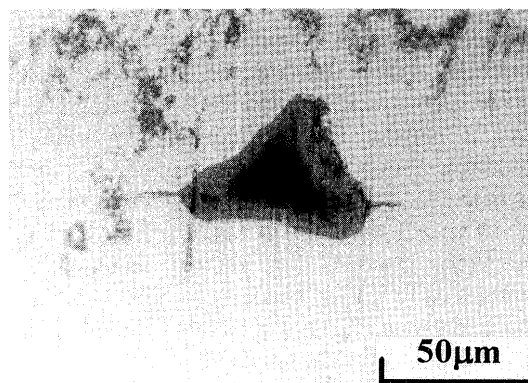


Fig.6. A crack initiated from a defect (Test 2). Stress axis is vertical.

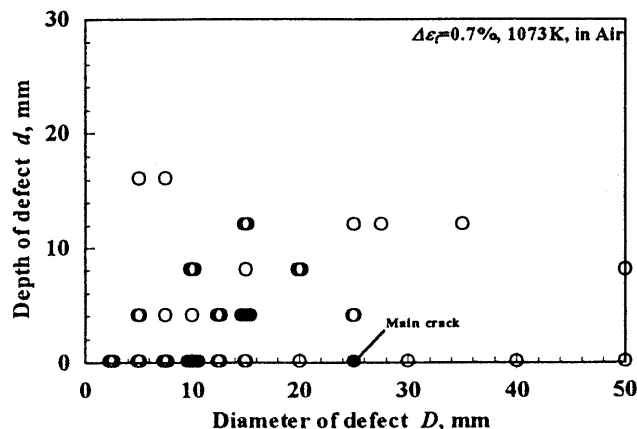


Fig.7. Diameter and depth of defects which involve the crack initiation (Test 2).

defined as the number of cracks per unit area on the specimen surface. The microcracks begin to initiate from very early stage of fatigue life. The first one appears at 100 cycles, which is less than 15% of life. The main crack, which brings about the failure of the specimen, comes from the incipient crack among all cracks observed. The density increases monotonically as the cycle increases, and it reaches 0.7mm^{-2} at the final failure. It is found that the crack density is larger as the (plastic) strain range is larger and the material is more ductile for some heat resistant steels [16,17]. For example, a type 304 stainless steel exhibits a high crack density of over 5mm^{-2} in LCF regime. It can be said that the LCF damage is characterized by the surface cracking with temporal and spatial distributions. As compared with ductile steels, however, the present TiAl permits a smaller amount of cracks, which might be attributed to the restriction of the plastic strain and the lack of the fracture toughness.

3.3. Growth of Microcracks

Figure 9 shows typical growth curves of microcracks. Since the crack density is low as shown in Fig.8, most of the microcracks grow without coalescence. They grow continuously while breaking the lamellae transversely. Figure 10 shows a magnified view of the crack, which displays a zigzag feature accompanied with partial delamination along the lamellar boundaries. Temporary arrests in the growth shown later might be attributed to the change of growth direction at the lamellar boundaries. In the previous study, the authors conducted room temperature (RT) fatigue of the same TiAl [12,13], which was more brittle at RT than at 1073K. The microcracks in the RT fatigue were accompanied with more distinct delamination than those in the present high temperature fatigue, whereby the crack-tip branching occurred frequently in the early stage of microcrack growth.

Figure 11 shows the morphology of initiation and growth process of a microcrack. The hatched part in the sketches show the casting defect. The crack grows smoothly as shown in Fig.9. It is not arrested at the grain boundary which is indicated by a broken line in the sketches of Fig.11. It has been reported that the growth of microcrack is often affected by grain boundary [18]. However, the grains of the present material are so large and the microcracks encountering grain boundaries become so long that the cracks break through the grain boundaries without interruption by the increasing stress intensity at the crack tip. Thus, neither grain boundaries nor lamellar boundaries drastically decelerate the microcrack growth.

Figure 12 shows the crack growth rate, dc/dN , as a function of the half crack length, c , for all cracks observed, where c is the crack length measured at the specimen surface. Although the growth rate disperses for an equal

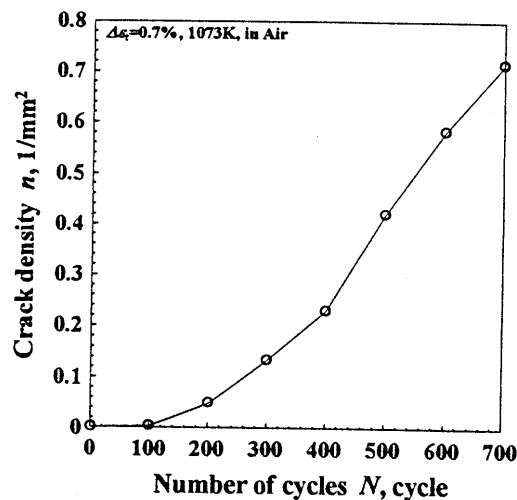


Fig.8. Change in crack density (Test 2).

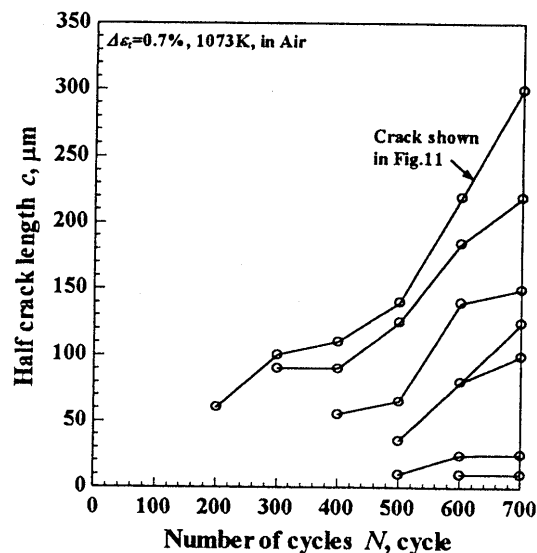


Fig.9. Typical crack growth curves (Test 2).

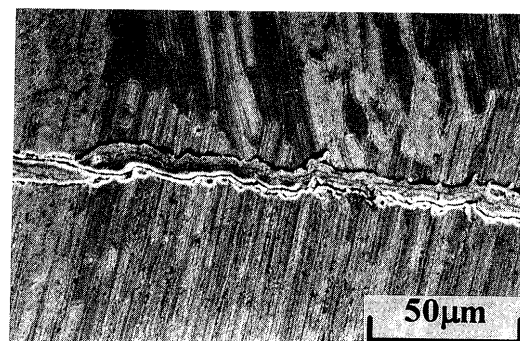


Fig.10. Feature of a microcrack growing transversely to the lamellae (Test 2). Stress axis is vertical.

MICROCRACKING AND LIFE LAW OF FATIGUE IN A CAST TiAl

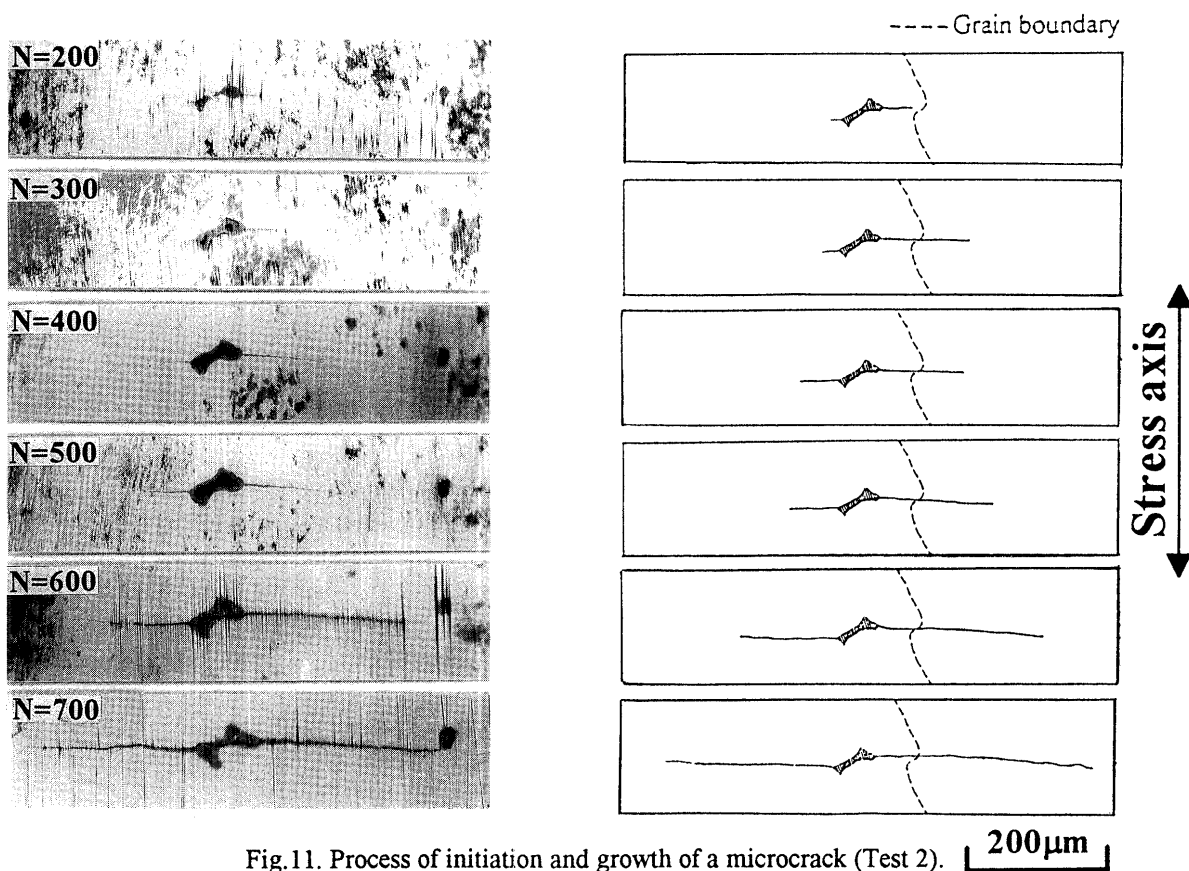


Fig.11. Process of initiation and growth of a microcrack (Test 2).

value of c , it tends to converge to a narrow band as the cracks become large. The fluctuation diminishes because the stress intensity for a long crack overcomes the disturbance due to the microstructure [17].

It was found in the previous study that the growth rate of a macrocrack, of which half length was over 2mm was correlated with the fatigue J-integral range, ΔJ_f [14]. Here, ΔJ_f is derived on the basis of a nonlinear fracture mechanics concept, and it represents the intensity of stress range in the vicinity of the crack tip in the elasto-plastic fatigue conditions [17, 19-21]. The value of ΔJ_f for a small crack in a homogeneous infinite body is evaluated by

$$\Delta J_f = 2\pi M_f \left\{ \frac{\Delta\sigma\Delta\varepsilon_e}{2} + \frac{n+1}{2\pi} f(n) \frac{\Delta\sigma\Delta\varepsilon_p}{n+1} \right\} c, \quad (1)$$

where, M_f is the correction factor for crack shape, $\Delta\sigma$ is the stress range, $\Delta\varepsilon_e$ is the elastic strain range, $\Delta\varepsilon_p$ is the plastic strain range, n is the stress exponent of non-time-dependent plastic deformation and $f(n)$ is the function of n . Assuming that $n=5.4$ and the crack is a semi-circular shape, $M_f=0.506$, then ΔJ_f is calculated for the microcracks shown in Fig.12. Figure 13 shows the relationship between ΔJ_f and dc/dN . The experimental results for the through macrocrack [14] are also plotted by solid symbols for

comparison. The growth rate for the microcracks distribute around the $dc/dN-\Delta J_f$ macrocrack. Thus, the average growth rate of microcracks is represented by the same

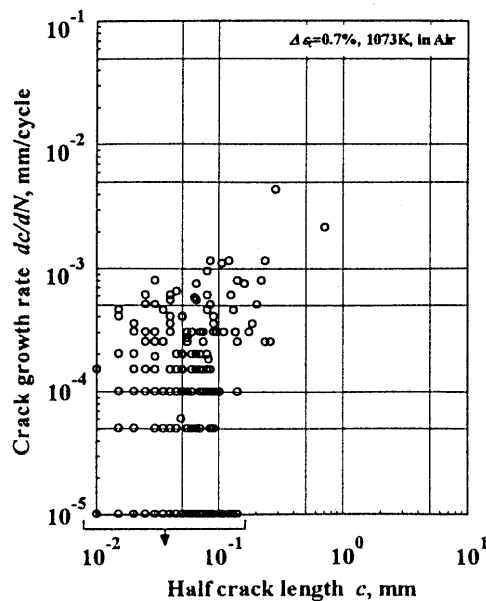


Fig.12. Relationship between growth rate and half crack length (Test 2).

fracture mechanics law. The relation is formulated as

$$dc/dN = C_f \Delta J_f^{m_f}, \quad (2)$$

where C_f and m_f are the material constants, and they are determined from the results of macrocrack growth tests at 1073K as 8.5×10^{-7} and 2.0, respectively, with dc/dN in m/cycle and ΔJ_f in kN/m.

3.4. $\Delta \tilde{W}_f$ -Parameter

By integrating Eq.(2) from c_0 to c_f , where c_0 and c_f are the crack lengths at the initiation and at the failure, respectively, the following is obtained.

$$\int_{c_0}^{c_f} \frac{dc}{C_f \Delta J_f} = \int_{N_i}^{N_f} dN, \quad (3)$$

where N_i is the crack initiation life. Substituting Eq.(2) into Eq.(3),

$$N_f - N_i = \int_{c_0}^{c_f} \frac{dc}{C_f \left[2\pi M_J \left\{ \frac{\Delta\sigma\Delta\varepsilon_e}{2} + \frac{n+1}{2\pi} f(n) \frac{\Delta\sigma\Delta\varepsilon_p}{n+1} \right\} c \right]}. \quad (4)$$

Since the main crack initiates at the very early stage of life in this study, the crack initiation life, N_i , can approximate to zero. Therefore, Eq.(4) leads to the following fatigue life

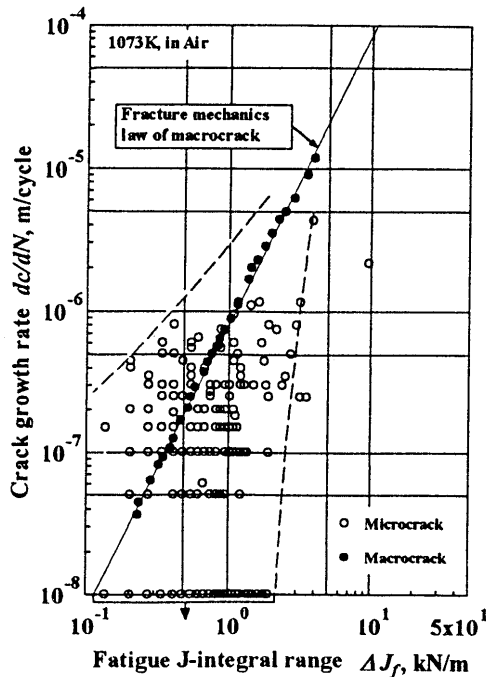


Fig. 13. Relationship between growth rate and fatigue J-integral range.

law [22, 23].

$$(\Delta \tilde{W}_f)^{m_f} N_f = D_f, \quad (5)$$

where

$$\Delta \tilde{W}_f = \frac{\Delta\sigma\Delta\varepsilon_e}{2} + \frac{n+1}{2\pi} f(n) \frac{\Delta\sigma\Delta\varepsilon_p}{n+1} \quad (6)$$

and

$$D_f = \frac{1}{C_f (2\pi M_J)^{m_f}} \frac{c_0^{-m_f+1} - c_f^{-m_f+1}}{m_f - 1} \quad (m_f \neq 1). \quad (7)$$

The $\Delta \tilde{W}_f$ -parameter has a dimension in the strain energy and correlates directly with ΔJ_f as

$$\Delta J_f = 2\pi M_J \Delta \tilde{W}_f c. \quad (8)$$

D_f is a constant when c_0 and c_f are determined and M_J is fixed.

Figure 14 shows the relationship between $\Delta \tilde{W}_f$ and N_f where the values of $\Delta \tilde{W}_f$ for the circular symbols are evaluated by substituting the measured stress range and strain ranges (see Table 2) into Eq.(6). The fatigue lives are linearly correlated well with the $\Delta \tilde{W}_f$ -parameter in the log-log plot. The straight line in Fig.14 is not a best fit of the circular symbols but shows the predicted relation on the basis of Eq.(5), where c_0 and c_f are assumed as 10 μ m and 1mm, respectively, based on the experimental observation of microcracks. Figure 14 indicates that the predicted relation corresponds considerably well with the experimental results in not only Test 2 (for specimen B) but also Tests 1 and 3 (for specimen A). The effect of

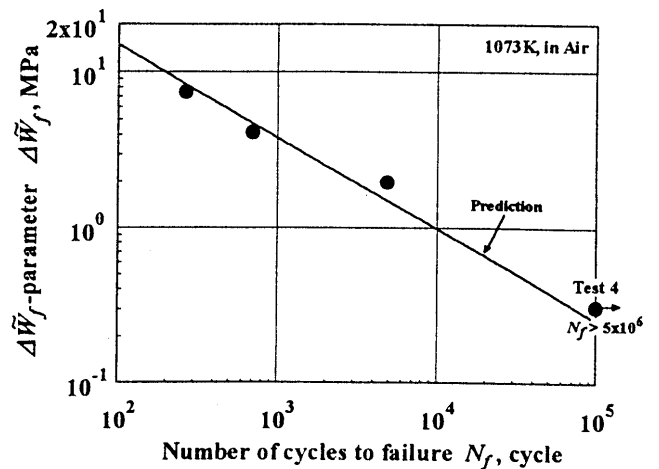


Fig. 14. Relationship between $\Delta \tilde{W}_f$ parameter and fatigue life. The line shows the prediction on the basis of Eq.(5).

MICROCRACKING AND LIFE LAW OF FATIGUE IN A CAST TiAl

specimen size can be negligible because the life law, Eq.(5), is insensitive to the value of c_f . The good correspondence confirms the validity of the life law of LCF in rather brittle materials as well as ductile steels and alloys reported previously [22, 23].

On the other hand, the predicted life for Test 4 is shorter than the actual one. In this case no crack is observed at the interruption at 5×10^6 cycles. This means that the crack initiation life in the TiAl cannot be negligible at lower strain range in high cycle fatigue just the same as the case of steels.

4. CONCLUSIONS

The characteristics of microcracks in a cast intermetallic compound, Ti-34wt.%Al, composed of the $\gamma+\alpha_2$ lamellar structure, were investigated under high temperature LCF conditions in order to elucidate the failure mechanism and mechanics. The results obtained are summarized as follows;

(1) The microcracks initiate from the cast defects at and/or beneath the surface.

(2) The incipient crack appears on the specimen surface at less than 15% of the fatigue life. It grows up to a main crack, which brings about the failure.

(3) Most microcracks grow rather continuously after the initiation while each of them shows an individual difference in the growth rate due to the microstructural effect. Although some of them are arrested temporarily at the lamellae and the grain boundaries, they break through the barrier soon.

(4) The growth rates of microcracks scatter around those of macrocracks which are correlated well with the fatigue J-integral range. As the microcrack grows, its rate converges to the fracture mechanics law represented by the relationship between crack growth rate and fatigue J-integral range for the macrocrack.

(5) Integrating the fracture mechanics law, $\Delta\tilde{W}_f$ -parameter is derived as a governing parameter of fatigue life, N_f . The predicted fatigue lives derived by the $\Delta\tilde{W}_f$ - N_f relation are in good correspondence with the actual ones. The life prediction based on the crack growth law is found to be valid for present TiAl.

Acknowledgments - This work was supported in part by Grant-in-Aids for Scientific Research of the Japanese Ministry of Education (Grant number 04239105 and 08455059) and Research Fellowships of Japan Society for the Promotion of Science for Young Scientists (Grant number 2-4110-6876). The authors would like to acknowledge Dr. T. Noda of Research and Development Division, Daido Steel Co., Ltd., for providing the material tested.

REFERENCES

1. Y-W. Kim, and, D. M. Dimiduk, Proc. 7th JIM Int. Symp., Japan Inst. Metals (1993) 373.
2. S. Mitao, S. Tsuyama, and K. Minakawa, Mater. Sci. Eng., **A143** (1991) 51.
3. M. Tokizane, T. Hukami and T. Inaba, ISIJ International, **31** (1991) 1088.
4. M. Dahms, J. Seeger, W. Smarsly and B. Wildhagen, *ibid.*, 1093.
5. H. Inui, M. H. Oh, A. Nakamura and M. Yamaguchi, Acta Metal. Mater., **40** (1992) 3095.
6. A. Ueno, H. Kishimoto, T. Kondo and N. Usuyama, Proc. 7th Symp. on Fracture and Fracture Mechanics (in Japanese), Soc. Mater. Sci., Japan (1993) 1.
7. D. L. Davidson and J. B. Campbell, Metallurg. Trans. A, **24A** (1993) 1555.
8. H. Shibata, K. Tokaji, T. Ogawa and H. Shiota, Trans. Japan Soc. Mech. Engrs., Ser. A (in Japanese), **61** (1995) 1205.
9. T. Nakano, H. Yasuda and Y. Umakoshi, Tetsu-to-Hagane (in Japanese), **80** (1994) 469.
10. K. Yamaguchi, M. Shimodaira and S. Nishijima, *ibid.*, **78** (1992) 134.
11. R. Gnanamoorthy, Y. Mutoh, N. Masahashi and Y. Mizuhara, J. Soc. Mater. Sci., Japan (in Japanese), **45** (1996) 919.
12. M. Tsutsumi, R. Ohtani, T. Kitamura, S. Takano and T. Ohshima, J. Soc. Mater. Sci., Japan (in Japanese), **44** (1995) 769.
13. R. Ohtani, T. Kitamura and M. Tsutsumi, Proc. Asian Pacific Conference for Fracture and Strength '96, Korean Soc. Mech. Engrs. (1996) 271.
14. M. Tsutsumi, S. Takano, T. Kitamura and R. Ohtani, Intermetallics, **4** (1996) 77.
15. S. Mitao, T. Isawa and S. Tsuyama, Scripta Metall. Mater., **26** (1992) 1405
16. R. Ohtani, T. Kitamura and N. Tada, Mater. Sci. Eng., **A143** (1991) 213.
17. R. Ohtani and T. Kitamura, Handbook of Fatigue Crack Propagation in Metallic Structures (ed. A. Carpinteri), Elsevier, **2** (1994) p.1347.
18. K. Tokaji and T. Ogawa, Short Fatigue Cracks (ed. by K. J. Miller and E. R. de los Rios), Mech. Eng. Publ. Ltd. (1992) p.85.
19. N. E. Dowling and J. A. Begley, ASTM STP 590 (1976) 82.
20. S. Taira, K. Tanaka and S. Ogawa, J. Soc. Mater. Sci., Japan (in Japanese), **26** (1977) 93.
21. S. Taira, R. Ohtani and T. Komatsu, Trans. ASME, J. Eng. Mater. Tech., **101** (1979) 162.
22. R. Ohtani and T. Kitamura, J. Soc. Mater. Sci., Japan (in Japanese), **34** (1985) 843.
23. R. Ohtani, T. Kitamura, A. Nitta and K. Kawabata, ASTM STP 942 (1987) 1163.